

Synthesis and Characterization of Pyridine-containing Epoxy: H-bonds Distribution and Thermomechanical Performances

ZHAO JUN,^a LIU AIQIN,^a ZHOU HONG,^a LUO JUN,^{*b} AND LIU YUAN^{*b}

^a Shanghai Space Propulsion Technology Research Institute, No. 1777, Zhongchun Road, Minhang District, Shanghai 201100 (P. R. China).

^b Engineering Research Center for Materials Protection of Wear and Corrosion of Guizhou Province, Guiyang University, Guiyang 550005 (P. R. China).

ABSTRACT

Heteroatoms (N, O, and F) and hydrogen groups are important elements for forming the H-bonds. It is well known that a large number of hydrogen groups are formed after curing reaction of epoxy. However, literatures about epoxy resins containing heteroaromatic ring and the H-bonds after cure reaction of the epoxy resins are seldom published. To bridge the gap, a kind of new epoxy monomer containing pyridine ring (EMP) has been synthesized in this work, and it is further cured by 4,4-diaminodiphenyl methane (DDM). The properties of cured EMP/DDM are evaluated by DSC, DMA, and static contact angle measurement. Moreover, the formation and the role of H-bonds in EMP/DDM are characterized by temperature-dependent FT-IR. The results show that the nitrogen heteroatom in pyridine ring effectively involves in the H-bonds and contributes a lot to the thermo-mechanical performances of cured EMP/DDM. We hope that the results presented in this work can work as a meaningful guide for utilization of the H-bonds to regulate the properties of epoxy resin.

KEYWORDS: Epoxy, H-bonds, properties, Temperature-dependent fourier transform infrared.

1. INTRODUCTION

Along with the booming of the industrialization in past three decades, thermosetting resins have gained wide variety of applications in

numerous industrial fields, such as aerospace, automotive, etc.^[1,2]. As a prominent example of such materials, epoxy resins have been becoming an integral part both in traditional

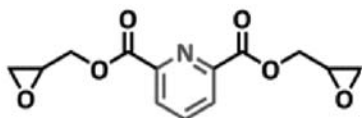
and nascent industrial fields, such as adhesives², electronic package^[3], 3D printing^[4], surface coatings^[5], etc., The nature of the precursors determines the network morphology of the cured epoxy resins, which, in turn, dictates the properties of the final thermosets. For this reason, careful design of the chemical structures of the epoxy precursors is the first prerequisite for understanding the fundamental characteristics of the cured resins, and the most feasible approach to achieving the goal is to fabricate model epoxy monomers, because the influences of the uncorrelated factor can be readily ruled out by building the model compounds appropriately.

In chemical substances containing strong electronegative atoms such as nitrogen, oxygen, etc., in addition to the direct interaction with its bonded atom, a hydrogen atom is also probably attracted by relatively strong force to electronegative atom, leading to an extra bond-like interaction between them, which is called H-bond^[6]. H-bond is one of crucial contributors to adhesive properties of thermosets^[7], and the H-bond between a hydroxyl group and a heteroatom is the most frequently reported one, for instance, Cheng and coworkers identified that the strength of H-bonds weakened when the H-bond of C=S...O-H substituted for C=O...O-H^[8]. Moreover, with the bond-like nature, H-bond is often used to improve the properties of the polymers, as discussed by Hobbie and coworkers, the miscibility of polystyrene/poly(butyl methacrylate) blends was enhanced by grafting hydroxy groups on the polystyrene, which could form H-bonds with the carbonyl groups in poly(butyl methacrylate). It is well known that a large quantity of hydroxyl groups

is formed after polymerization of the epoxy precursors, and naturally many a research sets forth to improving the properties of epoxy resins by constructing H-bond systems with these hydrogen groups. For example, Su et al. revealed that the H-bonds improved the miscibility of epoxy-benzoxazine/PEO-*b*-PCL blends, which further improve the performances of obtained composite^[5]. Thus, it is easy to find that researches about regulation of H-bond systems by adding external hydrogen bond donor or acceptor has been extensively reported. However, systematic and comprehensive understanding of the influences of the intrinsic H-bond systems both on curing behaviors of epoxy precursors and properties of cured thermosets, as well as the transitions of such H-bonds system, to the best of our knowledge, is still in a barren state. Therefore, it is necessary but also urgent to clarify the relationship between the properties of epoxy resin and its own intrinsic H-bond system. So far, our group have concerned with H-bond formation and hydrogen bonding types (*inter-* & *intra-*) in the polymers obtained by ring-opening polymerization, especially the ones containing heteroatoms^[9]. By focusing our attention on the mechanistic discussion of H-bond formation and the probably influences of H-bond on obtained thermosets, we found that the incorporation of heteroatoms into the benzoxazine monomer imposed a pronounced extra H-bond effect between the hydroxyl groups and the heteroatoms, which inspired us to further investigate the potential hydrogen bonding effect in epoxy resins, because a large number of hydroxyl groups are also formed in epoxy resins after the curing reaction.

In order to obtain more solid scientific evidences about the influences of the H-bonds on curing behaviors of epoxy precursors and on properties of corresponding cured networks, herein, a novel model epoxy monomer (Scheme 1) was carefully synthesized from 2,6-pyridinedicarbonyl chloride, and moreover, normal epoxy resin (bisphenol A based epoxy resin, DGEBA) was used as an experimental control.

Scheme 1. Chemical structure of EMP model epoxy monomer



2. EXPERIMENTAL

2.1 Materials

2,6-pyridinedicarbonyl chloride (96%), glycidol (98%), triethylamine (99%), 4,4'-diaminodiphenylmethane (DDM, 99%) were obtained from Aladdin Chemical Reagent Co. (Shanghai, China). Dichloromethane (A.R. grade), chloroform (A.R. grade), and petroleum ether (A.R. grade) were purchased from Sinopharm Chemical Reagent Co., Ltd. (Shanghai, China). DGEBA (DER331) was purchased from The DOW Chemical Company. All of reagents were used without any further purification.

2.2 Synthesis of bis(oxiran-2-ylmethyl)pyridine-2,6-dicarboxylate (EMP)

37.0 g (500 mmol) of glycidol, 75.75 g (750 mmol) of triethylamine and 200 ml of dichloromethane were added into a 1000 ml round three-necked flask equipped with a constant-pressure dropping funnel, an inlet for high purity nitrogen gas and a mechanical stirrer. After the reactor was cooled down to -3°C by ice salt bath, 40.8 g (200 mmol) of 2,6-pyridinedicarbonyl chloride dissolved in 200 ml of dichloromethane was added into

the flask using a constant-pressure dropping funnel, and the temperature was maintained at -3°C for another 7 h after the 2,6-pyridinedicarbonyl chloride was completely added into the flask. A fine white colored powder was obtained after being precipitated in petroleum ether and dried at 30°C under vacuum (yield: 71%).

^1H NMR (DMSO-*d*₆, δ ppm): 8.32 (d, $J = 7.7$ Hz, 2H), 8.24 (dd, $J = 8.8, 6.6$ Hz, 1H), 4.74 (dd, $J = 12.3, 2.7$ Hz, 2H), 4.16 (dd, $J = 12.4, 6.6$ Hz, 2H), 3.38 (dq, $J = 6.9, 3.0$ Hz, 2H), 2.87 (t, $J = 4.7$ Hz, 2H), 2.77 (dd, $J = 5.1, 2.6$ Hz, 2H).

^{13}C NMR (DMSO-*d*₆, δ ppm): 164.26, 147.99, 139.87, 128.78, 66.81, 49.38, 44.41.

FT-IR (KBr), cm^{-1} : 3007 cm^{-1} (pyridine ring C-H), 2955 and 2929 cm^{-1} (oxirane ring C-H), 1717 cm^{-1} (C=O), 1442 cm^{-1} (pyridine ring C=N), 1318 cm^{-1} (ester C-O), 1291 and 829 cm^{-1} (oxirane group C-O-C), 910 cm^{-1} (oxirane ring).

HRMS (ESI⁺) m/z calculated for $[\text{C}_{13}\text{H}_{13}\text{NO}_6\text{H}]^+$: 279.07, Found: 280.0635.

2.3 Cure of EMP and DGEBA

The EMP or DGEBA was mixed with DDM at equal molar ratio, and the mixture was dissolved in a small amount of chloroform at room temperature. Then the mixture was transferred to a silicone mold and degassed under vacuum at 60°C for 30 min, followed by curing at 100, 120, 140, 160 and 180°C for 2 h respectively.

2.4 Characterization

Nuclear magnetic resonance (NMR) spectra were recorded on a Bruker AVANCE III 400MHz at room temperature using DMSO-*d*₆ as the solvent. Mass spectra were obtained on a SCIEX LC-Q-TOF 4600. Fourier transform infrared (FT-IR) spectra were recorded on a Thermo Scientific Nicolet iS30. For temperature-dependent FTIR, the cured epoxy resins were inserted into a heatable fixture which was adapted to the Nicolet iS30, and the data were collected immediately after holding at target temperature for 1 h. Differential scanning calorimetry (DSC) measurement was performed on a NETZSCH DSC 214 under protection of high purity nitrogen gas, and the curing kinetics was determined

by DSC at different heating rates of 5, 10, 15, and 20°C min⁻¹. Thermogravimetric analysis (TGA) was conducted on a Mettler-Toledo TGA/DSC1 thermogravimetric analyzer under high purity nitrogen gas. Dynamic thermomechanical analysis (DMA) was performed on a TA Instruments Q800 under the tensile mode at a frequency of 1 Hz with the amplitude of 2 μm. Tensile tests were carried out on an Instron 5567 machine with a stretching rate of 1 mm·min⁻¹ at room temperature, and the tensile strength is taken the average value of three splines. Static contact angle was determined by a Dataphysics OCA25 using pendant drop method at room temperature. Before the test, the cured EMP/DDM was polished carefully to rule out the influences of surface roughness. In order to evaluate the hydrophobicity of the cured epoxy networks, 2 μl of deionized water was dropped onto the surface of tested sample using a micropipette, and to ensure the accuracy of the test, the measurements were repeated for 3 times on different splines for each designed sample. Moreover, static contact angle study was also tested by 1 μl of diiodomethane (CH₂I₂) for 3 times on different splines for the same sample, and finally, the surface free energy and polarity of each sample was

determined by Harmonic mean equations^[10, 11]:

$$(1 + \cos \theta_1)\gamma_1 = 4\left(\frac{\gamma_1^d \gamma_s^d}{\gamma_1^d + \gamma_s^d} + \frac{\gamma_1^p \gamma_s^p}{\gamma_1^p + \gamma_s^p}\right)$$

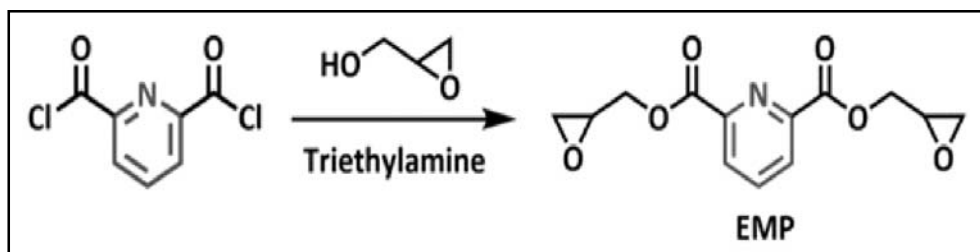
$$(1 + \cos \theta_2)\gamma_2 = 4\left(\frac{\gamma_2^d \gamma_s^d}{\gamma_2^d + \gamma_s^d} + \frac{\gamma_2^p \gamma_s^p}{\gamma_2^p + \gamma_s^p}\right)$$

where γ_s^d is the dispersive component, γ_s^p is the polar component; θ_1 is the contact angle to water; θ_2 is the contact angle to CH₂I₂; $\gamma_1 = 72.8$ mJ m⁻², $\gamma_2 = 50.8$ mJ m⁻², $\gamma_1^d = 22.1$ mJ m⁻², $\gamma_1^p = 50.7$ mJ m⁻², $\gamma_2^d = 44.1$ mJ m⁻², $\gamma_2^p = 6.7$ mJ m⁻².

RESULTS AND DISCUSSION

3.1 Design, Synthesis and Characterization of EMP.

According to Pascault J. P. *et al.*¹², there are usually three ways to prepare epoxy resins: (1) condensation reaction between phenolic hydroxyl group and excess epichlorohydrin in the aqueous solution of NaOH, however, with



Scheme 2. Synthetic route for EMP

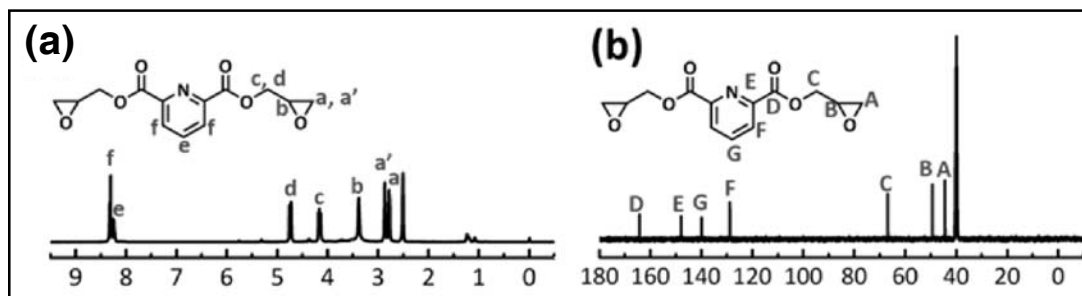


Fig. 1. NMR spectra of EMP: (a) ¹H NMR (b) ¹³C NMR.

this method, not the epoxy monomer but the oligomer is usually formed. For instance commercial diglycidyl ether of bisphenol A (DGEBA) prepared in this way generally contains 0.03~10 repeat units^[13]; (2) peroxidation of double carbon bond, and in our group's previous works^[14, 15], we successfully synthesized several bio-based epoxy monomers using this method; (3) The third method involves in a free radical initiated copolymerization of the glycidyl methacrylate (GMA) with other vinyl monomers. In this work, a novel synthesis route has been used to prepare high purity epoxy monomer, which involves in the reaction between chloride and glycidol (scheme 2). The chemical structure of

obtained epoxy monomer is firstly characterized by NMR (Figure 1). In the ¹H NMR, the three peaks locate at 2.5, 2.6 and 3.3 ppm (marked as a, a' and c) correspond to the three protons in oxirane groups^[16]. The peaks appear at 4.3 and 4.8 ppm (marked as c and d) are attributed to the protons of **-CH₂-** groups (Figure 1a). The two sets of peaks display at 8.3 and 8.4 ppm are ascribed to the aromatic protons on pyridine ring. The ¹³C NMR spectrum of EMP is exhibited in Figure 1b. As it is shown, the peaks at 42.3 and 49.7 ppm are attributed to the carbons in oxirane group, and signal at around 68.7 ppm corresponds to the carbons of **-CH₂-** group that connected to oxirane group^[17].

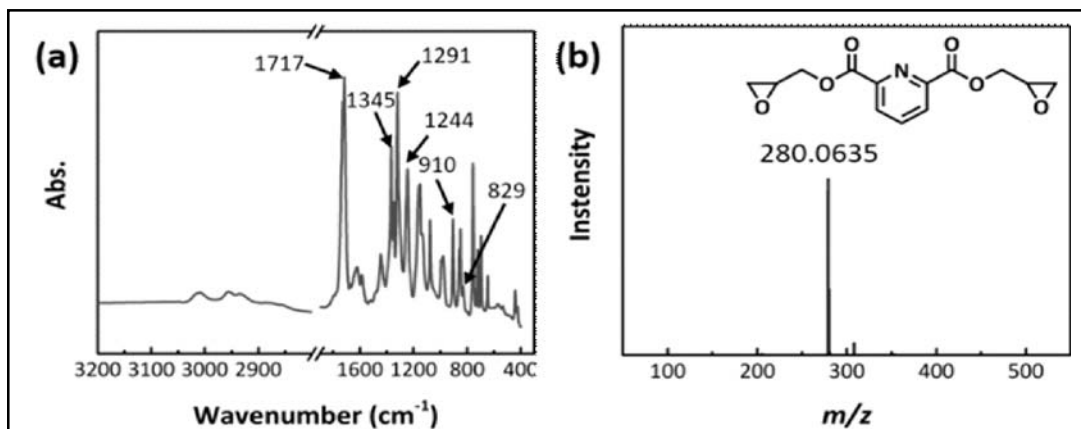


Fig. 2. FTIR and MASS spectra of EMP

FTIR was employed to further confirm the successful synthesis of EMP, and the obtained spectrum is shown in Figure 2a. The characteristic peaks locate at around 1291, 910 and 829 cm⁻¹ are ascribed to the stretching vibration of **C-O-C** and the breathing absorption in oxirane group, indicating the formation of oxirane group^[15, 18, 19]. Signals

display at around 1715 and 1250 cm⁻¹ correspond to the characteristic peak for symmetric stretching vibration of **C=O** and **C-O** in ester group (Figure 2a)^[20-22]. Note that, an apparent absorption peak at 1345 cm⁻¹ for aromatic amines is assigned to the stretching vibration of **C-N** in pyridine ring (Figure 2a)^[23]. Mass spectrum of obtained EMP is displayed in Figure 2b, and

only one significant singlet peak can be seen at 280 g mol⁻¹. Molecular weight result obtained from MALDI-TOF is in good agreement with the calculated data, suggesting the high purity of the synthesized EMP.

Melting point has been widely used in organic chemistry to evaluate the purity of prepared compound, and the purer of the compound, the sharper melting peak is^[24]. The melting temperatures of EMP was evaluated using a DSC (Figure S1), and the sharp melting peak indicates the purity of EMP is satisfied.

3.2 Curing behavior and kinetics of the EMP/DDM and DGEBA/DDM.

Obviously, regardless of the heating rates, only one exothermic peak appears in each curve (Figure 3a and 3c). The presence of the exothermic peak is due to the fact that the epoxy groups undergo ring-opening polymerization. To make a quantitative evaluation of curing reaction, Kissinger (eq. 1) and Ozawa (eq. 2) methods are applied to calculate polymerization reaction kinetic parameters^[25, 26].

$$\ln \frac{\beta}{T_p^2} = \ln \frac{AR}{E} - \frac{E}{RT_p} \quad (\text{eq. 1})$$

$$\ln \beta - \frac{E}{RT_p} = 1.052 \frac{E}{RT_p} + C \quad (\text{eq. 2})$$

where T_p is the peak temperature (K), β is the heating rate (K min⁻¹), E is the activation energy (J mol⁻¹), A is the pre-exponential factor and R is the universal gas constant.

By measuring the exothermic peak temperatures (T_p) at heating rates of 5, 10, 15, and 20 K min⁻¹ (Figure 3a and 3c), several straight lines are obtained (Figure 3b and 3d), and the calculated E_a values for EMP/DDM are

42.4 kJ mol⁻¹ (Kissinger method) and 46.5 kJ mol⁻¹ (Ozawa method) and the E_a values for DGEBA/DDM are 35.4 kJ mol⁻¹ (Kissinger method) and 40.5 kJ mol⁻¹ (Ozawa method) respectively. Note that, although the E_a value of DGEBA/DDM is lower than that of EMP/DDM, the peak temperatures of EMP/DDM are lower than those of DGEBA/DDM in all heating rates. This is probably due to the catalysis effect of the H -bonds on curing reaction of the EMP, which has been widely proved by curing of other thermosets^[25].

Fig. 3. (a) Plots obtained from DSC thermograms of EMP/DDM at different heating rates of 5 °C min⁻¹, 10 °C min⁻¹, 15 °C min⁻¹ and 20 °C min⁻¹; (b) linear plots obtained by Kissinger method (solidline) and Ozawa method (dashed line) of EMP/DDM; (c) plots obtained from DSC thermograms of DGEBA/DDM at different heating rates of 5 °C min⁻¹, 10 °C min⁻¹, 15 °C min⁻¹ and 20 °C min⁻¹; (d) linear plots obtained by Kissinger method (solidline) and Ozawa method (dashed line) of DGEBA/DDM.

3.3 Dynamic mechanical properties of cured EMP/DDM and DGEBA/DDM.

The synthesized EMP and commercial obtained DGEBA were cured by amine-based curing agent DDM in the curing procedures of 100, 120, 140, 160 and 180 °C for 2 h respectively. To ensure the synthesized epoxy monomer and DGEBA have been fully cured under this condition, and to further guarantee the accuracy of the data obtained from DMA test, we firstly used DSC to inspect the completeness of the curing reaction (Figure S2). As it is shown, two almost horizontal lines are observed in the temperature range of

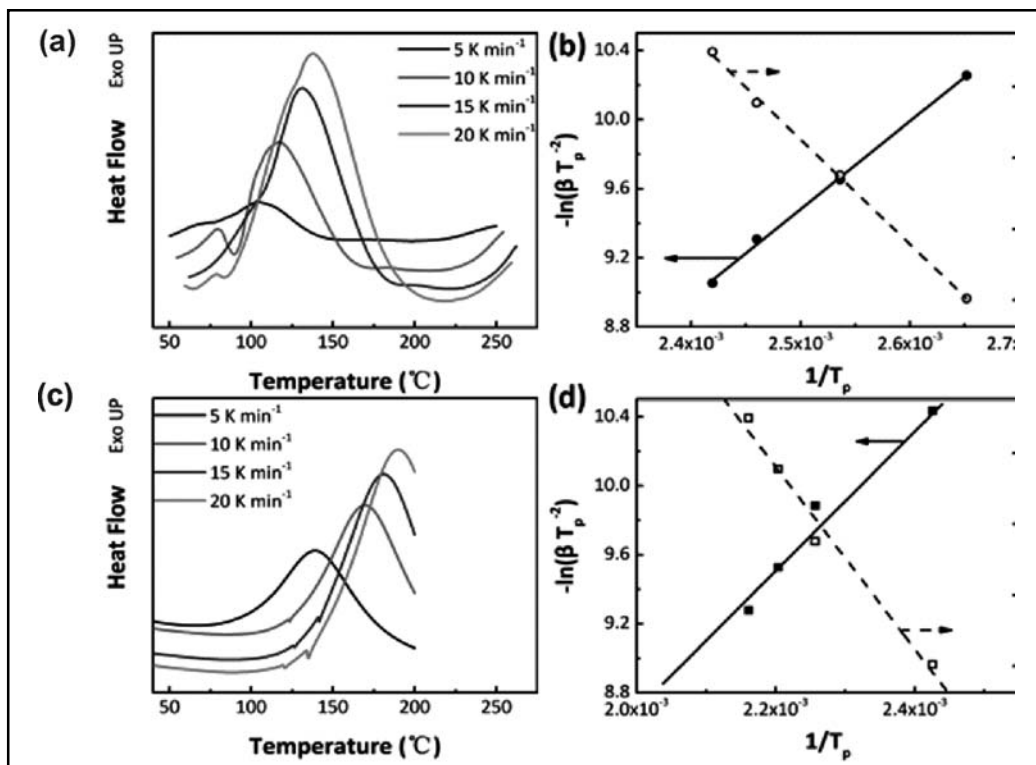


Fig. 3. DMA curves of cured EMP/DDM and DGEBA/DDM: (a) storage modulus as a function of temperature; (b) $\tan \delta$ as a function of temperature.

20-200°C, and neither exothermic nor endothermic peak is observed in the Figure S2, indicating the completeness of the curing reactions.

Dynamic mechanical properties of the cured EMP/DDM and DGEBA/DDM were analyzed by using DMA. As can be seen, one-step decrease of the storage modulus is presented both in EMP/DDM and DGEBA/DDM in Figure 3a, which can further be proved by the single peak in its corresponding $\tan \delta$ curve (Figure 3b). The storage modulus values of EMP/DDM and DGEBA/DDM are 2.1 and 2.7 Gpa, respectively at room temperature, and the glass

transition temperatures (T_g) of EMP/DDM and DGEBA/DDM are determined by the peak temperature of the $\tan \delta$ versus temperature curve (Figure 3b), which are 124.4 and 149.1 °C, respectively. Interestingly, when the temperature is 180 °C, the storage modulus value of EMP/DDM is still as high as 15.6 MPa, whereas the storage modulus value of DGEBA/DDM is decreased to 3.7 MPa. Because the crosslink density plays an important role in determination of the storage modulus^[27], and thus we calculated the crosslinking density by equation (3) at first^[13]:

$$\nu_e = \frac{E'_R}{3RT} \quad (\text{eq. 3})$$

where the ν_e is the cross-linking density (mol dm^{-3}), E_R is the storage modulus recorded at $T_g+30^\circ\text{C}$, R is the gas constant, and T is the absolute temperature at $T_g+30^\circ\text{C}$. Moreover, the calculated values are 1.2 and 0.8 mol dm^{-3} .

3.4 Thermal Properties of EMP/DDM and DGEBA/DDM.

In order to have a better understanding of the thermal properties of cured EMP/DDM and

DGEBA/DDM, DSC and TGA were employed to evaluate the thermal stabilities of EMP/DDM and DGEBA/DDM. To ensure the accuracy of the results, the samples were subject to the pretreatment of thermal history elimination before their T_g values were evaluated using a DSC (Figure 4a). The parameters obtained from DSC and TGA analysis are summarized in Table 3.

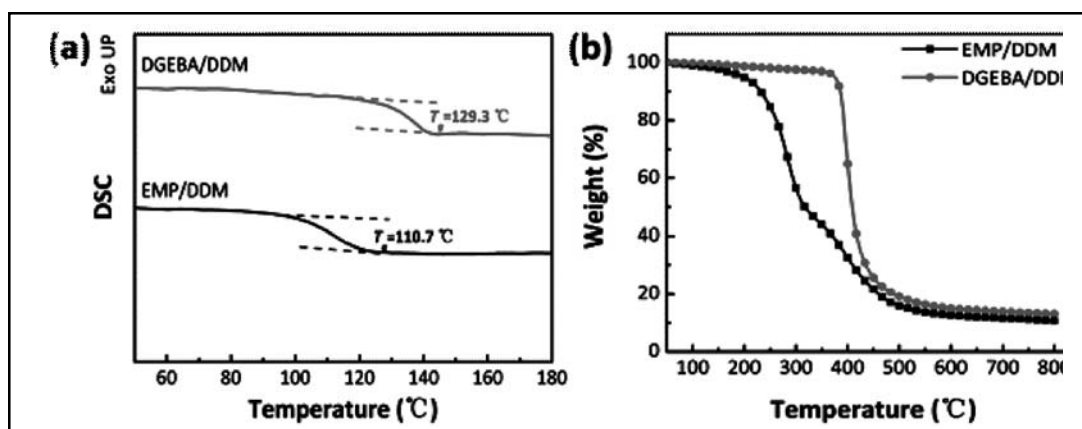


Fig. 4. (a) DSC thermograms of cured EMP/DDM and DGEBA/DDM; (b) TGA curves of cured EMP/DDM and DGEBA/DDM.

TABLE 3. Parameters obtained from the DSC and TGA

Samples	T_g from the DSC ($^\circ\text{C}$)	$T_{d,5\%}$ ($^\circ\text{C}$)	$T_{d,30\%}$ ($^\circ\text{C}$)	Char yield (@ 800°C)
EMP/DDM	110.7	197.0	409.3	10.6
DGEBA/DDM	129.3	375.7	423.1	13.2

Obviously, except for a parallel movement of the baseline toward the endothermic direction, there is no exothermic peak can be detected for EMP/DDM and DGEBA/DDM in the whole range of the heating scan (Figure 4a), suggesting the completeness of the curing

reactions again. As can be seen, the values of T_g are 110.7°C for EMP/DDM and 129.3°C for DGEBA/DDM. Thermal degradation processes of cured epoxy resins were inspected by TGA, and the result is recorded as mass losses versus temperature (Figure 4b). While the EMP/

DDM demonstrates a two-stage degradation process, the DGEBA/DDM exhibits one step thermal degradation. The EMP/DDM demonstrates a rather undesirable thermal stability with two distinct degradation stages with maximum rates at 283.0 and 400.1°C respectively. The poor thermal stability of EMP/DDM may be ascribed to the poor stability of the pyridine ring, which was mentioned in the

literature [28].

3.5 Mechanical properties of cured EMP/DDM and DGEBA/DDM.

The chemical structure of epoxy monomer and the curing agent have significant influences on mechanical performances of the cured network. The mechanical properties of cured EMP/DDM and DGEBA/DDM were appraised

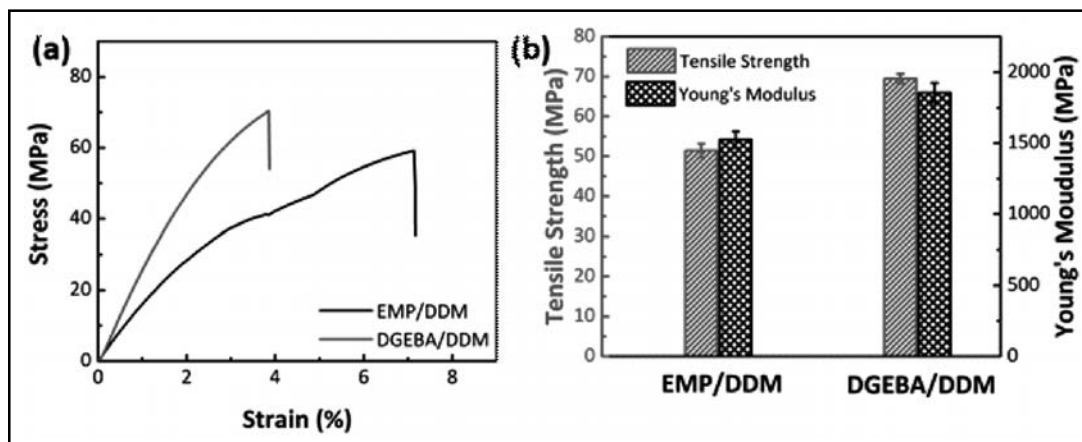


Fig. 5. Tensile properties of three cured epoxy networks: (a) stress-strain curves of one of tested samples; (b). tensile strength and Young's modulus.

by their tensile properties (Figure 5).

One of representative stress-strain curves for cured EMP/DDM and DGEBA/DDM are shown in Figure 5a. The tensile strength (average values) of cured EMP/DDM and DGEBA/DDM are presented in Figure 5b which are 51.4 MPa for EMP/DDM and 68.9 MPa for DGEBA/DDM; the Young's modulus are 1.5 GPa for EMP/DDM and 1.8 GPa for DGEBA/DDM. It should be noted that due to the presence of C-N=C in pyridine ring, more hydrogen bonds are formed accordingly after curing reaction,

which effectively enhance its mechanical performances, including the Young's modulus and tensile strength [29, 30]. However, its tensile strength is still lower than that of the DGEBA/DDM, and this is probably due to the fact that more rigid structures (benzene rings) are presented in the DGEBA, which can endow the epoxy with more excellent mechanical properties.

3.6 Contact angle analysis of cured EMP/DDM and DGEBA/DDM.

Chemical composition has an important role

in affecting the hydrophilicity/hydrophobicity of the polymer. As reported by Wang and coworkers, the polar groups can effectively improve the hydrophilicity of the polymer [11]. Thus, theoretically, compared with DGEBA/DDM, the EMP/DDM should demonstrate more hydrophilicity because the existence of the pyridine ring in EMP's chemical structure. To get more quantitative data about the

hydrophilicity/hydrophobicity of EMP/DDM and DGEBA/DDM, contact angles of the liquid droplet on the polished surfaces of cured DGEBA/DDM and EMP/DDM have been measured with two different liquids with varying surface tension (Figure 6), and the values of surface free energy of the DGEBA/DDM and EMP/DDM are calculated according to the Harmonic mean equations (Table 4).

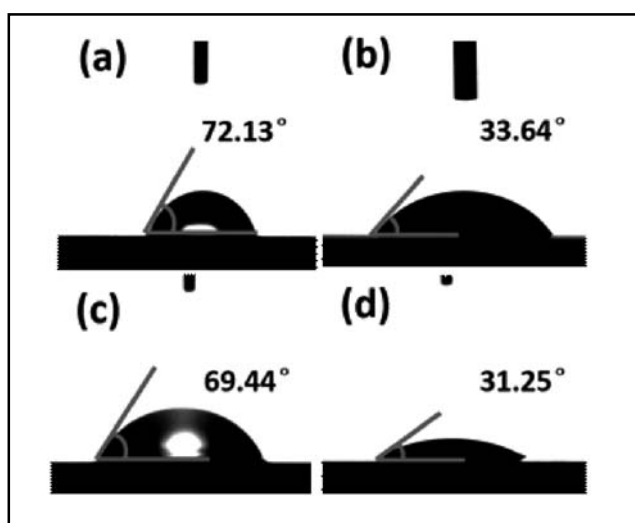


Fig. 6. Contact angle of cured EMP/DDM and DGEBA/DDM at room temperature: (a) water contact angle of DGEBA/DDM; (b) diiodomethane contact angle of DGEBA/DDM; (c) water contact angle of EMP/DDM; (d) diiodomethane contact angle of EMP/DDM.

TABLE 4. Contact angle and surface energy study of EMP/DDM and DGEBA/DDM.

Samples	$\theta_{\text{CH}_2\text{O}}$	$\theta_{\text{CH}_2\text{I}_2}$	Dispersive component (γ_s^d) (γ_s^p)	Polar component ($\gamma_s = \gamma_s^p + \gamma_s^d$)	Surface energy
EMP/DDM	69.44 ± 0.7	31.25 ± 0.8	36.6	14.1	50.7
DGEBA/DDM	72.13 ± 0.4	33.64 ± 0.5	32.9	29.6	62.5

Surprisingly, even though there are a large number of nitrogen atoms (in the pyridine rings) in cured EMP/DDM, the polar component (γ_s^p) of cured EMP/DDM is rather small, even smaller

than that of DGEBA/DDM. Naturally, the question arises what kind of fundamental reason is responsible for this unanticipated phenomenon? Based on above results and

analysis, especially the results obtained from the DMA and mechanical tests, we confidently speculate that varieties of H-bonds formed after curing reaction are the key factors influencing the cross-link densities, Young's modulus and hydrophilicity/hydrophobicity of cured EMP/DDM (Figure 7).

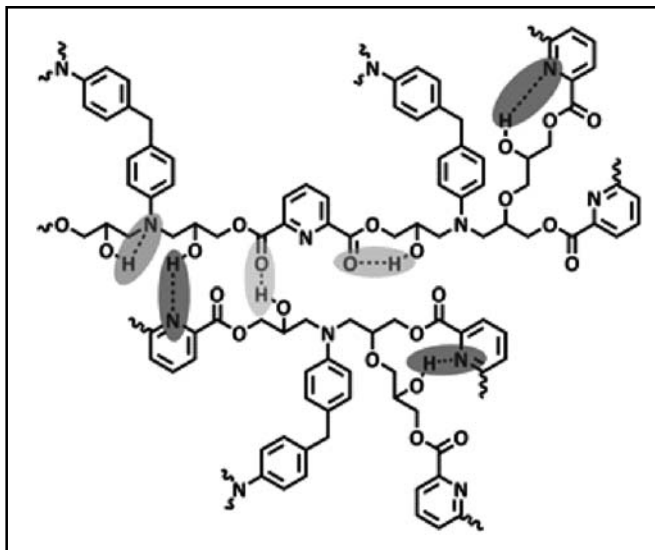


Fig. 7. Proposed distribution of H-bonds in EMP/DDM.

3.7 Temperature-dependent FT-IR analysis and proposed hydrogen bonding distribution in different cured EMP/DDM and DGEBA/DDM.

FT-IR is a powerful tool to obtain the information on hydrogen bonding, both qualitatively and quantitatively^[31]. In order to clarify the H-bonds in cured EMP/DDM and DGEBA/DDM, temperature-dependent FT-IR was conducted after keeping 1 h at RT, 90, 110, and 150 °C respectively, and the normalized spectra are displayed in Figure S3 and S4. As it is shown, A very broad band centered at around 3400 cm^{-1} can be attributed to the wide existence of the H-bonds in the cured EMP/DDM, which are resulted from the presence of the great amount

of the hydroxyl groups after the ring-opening polymerization of the epoxy groups^[32]. Moreover, the region of the cured EMP/DDM is larger than that of the cured DGEBA/DDM, indicating that more H-bonds formed in EMP/DDM than that of DGEBA/DDM. In addition, due to the redistribution of the hydroxyl group associations, a common phenomenon that the -OH stretching region changes apparently along with the increase of the temperature has also been observed in all cured networks.

To gather more detailed information about the rearrangements of the hydrogen bonding systems, we performed a curve fitting of the hydroxyl vibration region (Figure 8). The fitting results give 4 bands at around ~3536, ~3415,

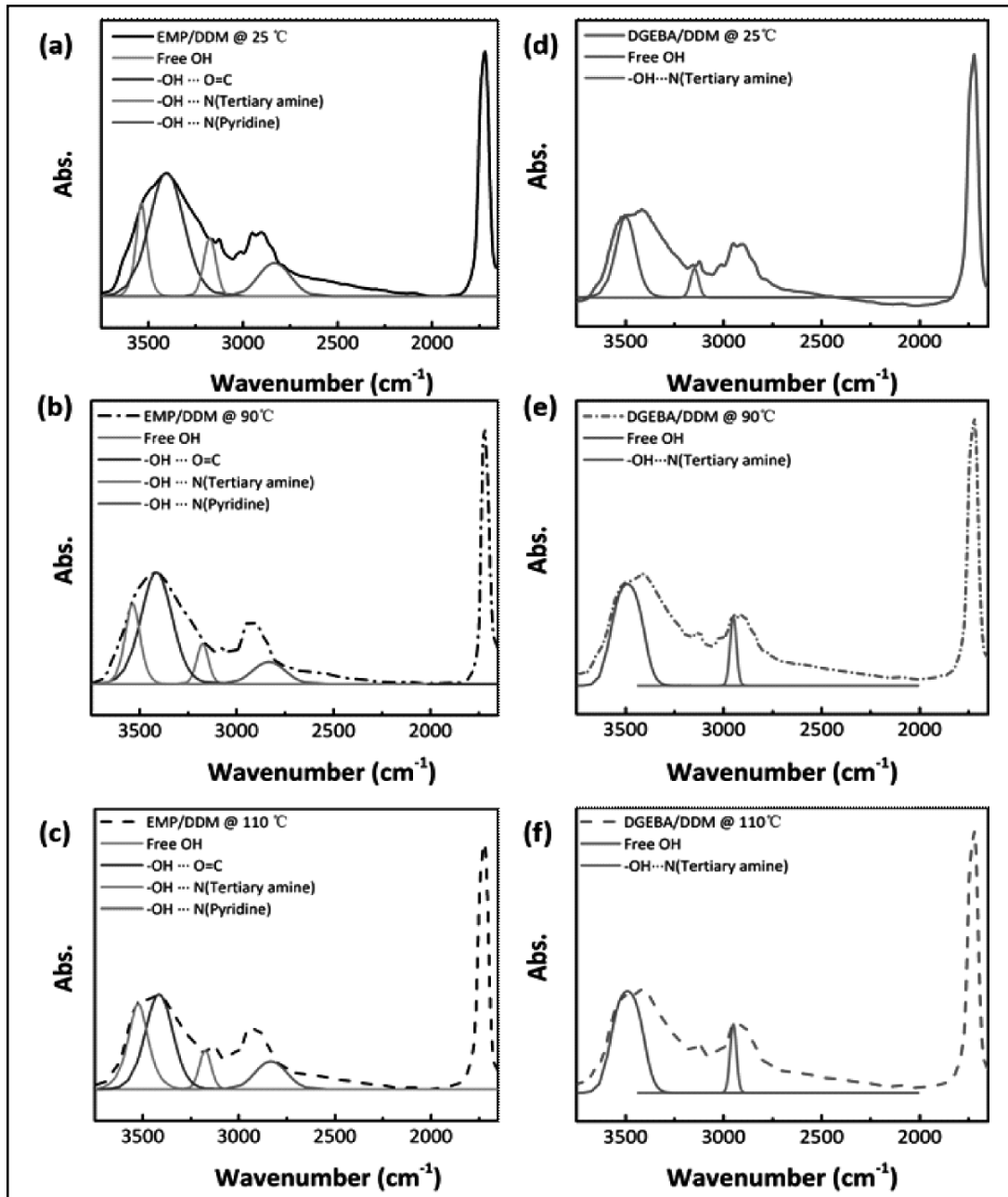


Figure 8. Typical curve fitting results of the H-bond regions of cured EMP/DDM and DGEBA/DDM: (a) EMP/DDM at 25 °C; (b) EMP/DDM at 90 °C; (c) EMP/DDM at 110 °C; (d) DGEBA/DDM at 25 °C; (e) DGEBA/DDM at 90 °C; (f) DGEBA/DDM at 110 °C.

~3175 and ~2833 cm^{-1} for cured EMP/DDM, whereas only 2 bands at around ~3536 and 2850 cm^{-1} are fitted for DGEBA/DDM. The bands located at around ~3415 cm^{-1} are assigned to hydrogen bonded hydroxyl groups and carbonyl groups, and the bands centered at ~3536 cm^{-1} are attributed to the appearance of the free hydroxyl groups^[31]. Thus, it can be seen that the DGEBA/DDM have more free hydrogen groups than the EMP/DDM. Moreover, the absorption bands at ~3175 cm^{-1} correspond to the association between hydroxyl groups and nitrogen atoms in alkylamine. Moreover, the H-bonds between hydroxyl groups and pyridyl groups in cured EMP/DDM can be directly confirmed from the appearance of the peak centered at around 2833 cm^{-1} ^[33].

4. CONCLUSIONS

Novel epoxy monomer EMP containing pyridyl group has been carefully synthesized to evaluate the effects of H-bonds on properties of cured epoxy resin. The DMA and contact angle measurement demonstrate varieties of hydrogen bonding systems formed after curing reaction, and the temperature-dependent FT-IR analysis confirms that H-bonds formed between the hydrogen group and the pyridyl groups, which further endows the cured EMP/DDM with relatively low surface energy value and better performances of thermal properties.

ASSOCIATED CONTENT

Supporting Information

Melting temperatures of three epoxy monomers (Figure S1), confirmation of the completeness of the curing reaction (Figure S2), temperature-dependent FT-IR spectra of EMP/DDM (Figure

S3), temperature-dependent FT-IR spectra of DGEBA/DDM (Figure S4).

REFERENCES

1. Finzel, M. C., Delong, J., Hawley, M. C., *Journal of Polymer Science: Part A Polymer Chemistry* 1995, 33(4), 673-689.
2. Mijovic, J., Fishbain, A., Wijaya, J., *Macromolecules* 1992, 25(2), 979-985.
3. Liu, Y., Dai, J., Liu, X., Luo, J., You, S., Zhu, J., Ma, S., Jia, Z., *Journal of Electronic Packaging* 2017, 139(3), 031006.
4. Yu, R., Yang, X., Zhang, Y., Zhao, X., Wu, X., Zhao, T., Zhao, Y., Huang, W., *ACS Applied Materials & Interfaces* 2017, 9(2), 1820-1829.
5. Su, W. C., Tsai, F. C., Huang, C. F., Dai, L., Kuo, S. W., *Polymers (Basel)* 2019, 11(2), 201.
6. Zhang, W., Dehghani-Sanij, A. A., Blackburn, R. S., IR Study on Hydrogen Bonding in Epoxy Resin-Silica Nanocomposites. *Progress in Natural Science* 2008, 18(7), 801-805.
7. Snow, A. W., Armistead, J. P., *The Journal of Adhesion* 1995, 52(1), 223-250.
8. Cheng, Y., Zhang, X., Zhang, W., *Heteroatom Chemistry* 2013, 24(3), 153-162.
9. Shen, X., Cao, L., Liu, Y., Dai, J., Liu, X., Zhu, J., Du, S., *Macromolecules* 2018, 51(13), 4782-4799.
10. Ou, W., Qiu, H., Chen, Z., Xu, K., *Biomaterials* 2011, 32(12), 3178-88.
11. Yang, J., Bei, J., Wang, S., *Biomaterials* 2002, 23(12), 2607-2614.
12. Auvergne, R., Caillol, S., David, G., Boutevin, B., Pascault, J. P., *Chemical Reviews* 2014, 114(2), 1082-1115.
13. Miao, J.T., Yuan, L., Guan, Q., Liang, G., Gu, A., *ACS Sustainable Chemistry & Engineering* 2017, 5(8), 7003-7011.

14. Ma, S., Liu, X., Jiang, Y., Fan, L., Feng, J., Zhu, J., *Science China Chemistry* 2013, 57(3), 379-388.
15. Deng, J., Liu, X., Li, C., Jiang, Y., Zhu, J., *Rsc Advances* 2015, 5(21), 15930-15939.
16. Aouf, C., Nouailhas, H., Fache, M., Caillol, S., Boutevin, B., Fulcrand, H., *European Polymer Journal* 2013, 49(6), 1185-1195.
17. Chrysanthos, M., Galy, J., Pascault, J.P., *Polymer* 2011, 52(16), 3611-3620.
18. Nikafshar, S., Zabihi, O., Hamidi, S., Moradi, Y., Barzegar, S., Ahmadi, M., Naebe, M., *A Renewable RSC Advances* 2017, 7(14), 8694-8701.
19. Chen, J., Li, X., Wang, Y., Huang, J., Li, K., Nie, X., Jiang, J., *European Journal of Lipid Science and Technology* 2017, 119(5), 1600216.
20. Liu, Y. L., Hsieh, C. Y., *Journal of Polymer Science Part A: Polymer Chemistry* 2006, 44(2), 905-913.
21. Nishikubo, T., Shimokawa, T., Hirano, T., Shiina, A., *Journal of Polymer Science Part A: Polymer Chemistry* 1989, 27(8), 2519-2530.
22. Zhang, K., Huang, C., Fang, Q., Lu, Q., *Journal of Applied Polymer Science* 2017, 134(6), 44246.
23. Sundaraganesan, N., Kalaichelvan, S., Meganathan, C., Joshua, B. D., Cornard, J., *Spectrochim Acta A Mol Biomol Spectrosc* 2008, 71(3), 898-906.
24. Aston, J. G., Fink, H. L., Tooke, J. W., Cines, M. R., *Analytical Chemistry* 1947, 19(4), 218-221.
25. Shen, X. B., Liu, X. Q., Dai, J. Y., Liu, Y., Zhang, Y. J., Zhu, J., *Industrial & Engineering Chemistry Research* 2017, 56(38), 10929-10938.
26. Jia, Q. M., Zheng, M., Zhu, Y. C., Li, J. B., Xu, C. Z., *European Polymer Journal* 2007, 43(1), 35-42.
27. Xia, Y., Larock, R. C., *Polymer* 2010, 51(12), 2508-2514.
28. Heinicke, J., Oprea, A., Kindermann, M. K., Karpati, T., Nyulászi, L., Veszprémi, T., *Chemistry – A European Journal* 1998, 4(3), 541-545.
29. Su, E., Yurtsever, M., Okay, O., *Macromolecules* 2019, 52(9), 3257-3267.
30. Tashiro, K., Kobayashi, M., *Polymer* 1991, 32(8), 1516-1526.
31. Kuo, S. W., Huang, C. F., Chang, F. C., *Journal of Polymer Science Part B: Polymer Physics* 2001, 39(12), 1348-1359.
32. Mikhaylova, Y., Adam, G., Häußler, L., Eichhorn, K. J., Voit, B., *Journal of Molecular Structure* 2006, 788(1-3), 80-88.
33. He, W., Pan, G., Yang, Z., Zhao, D., Niu, G., Huang, W., Yuan, X., Guo, J., Cao, H., Yang, H., *Advanced Materials* 2009, 21(20), 2050-2053.

Received: 20-12-2019

Accepted: 28-01-2020